

# Retuning the Catalytic Bias and Overpotential of a [NiFe]-Hydrogenase via a Single Amino Acid Exchange at the Electron Entry/Exit Site

Hope Adamson,<sup>†,‡</sup> Martin Robinson,<sup>‡</sup> John J. Wright,<sup>§</sup> Lindsey A. Flanagan,<sup>†</sup> Julia Walton,<sup>†</sup> Darrell Elton,<sup>||</sup> David J. Gavaghan,<sup>‡</sup> Alan M. Bond,<sup>⊥</sup> Maxie M. Roessler,<sup>§</sup> and Alison Parkin<sup>\*,†,||</sup>

<sup>†</sup>Department of Chemistry, University of York, Heslington, York YO10 5DD, U.K.

<sup>‡</sup>Department of Computer Science, University of Oxford, Oxford, OX1 3QD, U.K.

<sup>§</sup>School of Biological and Chemical Sciences, Queen Mary University of London, Mile End Road, London, E1 4NS, U.K.

<sup>||</sup>Department of Engineering, School of Engineering and Mathematical Sciences, La Trobe University, Melbourne, Victoria 3086, Australia

<sup>⊥</sup>School of Chemistry, Monash University, Clayton, Victoria 3800, Australia

## Supporting Information

**ABSTRACT:** The redox chemistry of the electron entry/exit site in *Escherichia coli* hydrogenase-1 is shown to play a vital role in tuning biocatalysis. Inspired by nature, we generate a HyaA-R193L variant to disrupt a proposed Arg–His cation– $\pi$  interaction in the secondary coordination sphere of the outermost, “distal”, iron–sulfur cluster. This rewires the enzyme, enhancing the relative rate of  $H_2$  production and the thermodynamic efficiency of  $H_2$  oxidation catalysis. On the basis of Fourier transformed alternating current voltammetry measurements, we relate these changes in catalysis to a shift in the distal  $[Fe_4S_4]^{2+/1+}$  redox potential, a previously experimentally inaccessible parameter. Thus, metalloenzyme chemistry is shown to be tuned by the second coordination sphere of an electron transfer site distant from the catalytic center.

## INTRODUCTION

Hydrogenases are remarkable biological catalysts, with the ability to interconvert  $H_2$ , protons, and electrons ( $H_2 \rightleftharpoons 2H^+ + 2e^-$ ) at rates comparable to platinum, but using abundant-metal active sites of iron or nickel and iron.<sup>1</sup> These enzymes are therefore studied with the hope of both understanding microbial metabolism and discovering sustainable catalysts to underpin a  $H_2$ -energy economy. The  $O_2$ -tolerant membrane-bound [NiFe]-hydrogenases (MBHs), capable of sustained catalysis in  $O_2$ , have garnered the most significant interest (Figure 1a). Reprogramming the reactivity of such [NiFe]-hydrogenases is desirable because there is not a naturally occurring enzyme that is both active in  $O_2$  and capable of high-efficiency catalysis and rapid  $H_2$  production. This is particularly clear in catalytic protein film voltammetry experiments, in which hydrogenase is adsorbed onto the surface of an electrode and catalytic current is measured as a function of potential, fingerprinting both the catalytic bias (ratio of  $H_2$  oxidation to  $H_2$  production current) and the potential at which catalysis commences (Figure 1b).<sup>2,3</sup> The [NiFe]-hydrogenases that are ideal bidirectional  $H_2$  electrocatalysts, displaying high  $H_2$  production and oxidation turnover rates, are inactivated by  $O_2$  ( $O_2$ -sensitive, e.g., *Escherichia coli* hydrogenase-2).<sup>2,4,5</sup>

Conversely, the  $O_2$ -tolerant MBHs are poor  $H_2$ -producing catalysts and require an additional thermodynamic driving force (overpotential) to initiate  $H_2$  oxidation at pH > 5, e.g., *Escherichia coli* hydrogenase-1 (*E. coli* Hyd-1).<sup>2,4,5</sup> Therefore, despite [NiFe]-hydrogenases being naturally expressed by photosynthetic microbes,<sup>6</sup> sustained solar water-splitting to yield  $H_2$  is impossible using native enzymes, and a molecular understanding of the factors that control catalytic bias and overpotential is required.

Crystal structures have been resolved for four  $O_2$ -tolerant MBHs, including the subject of this study, *E. coli* Hyd-1.<sup>7–12</sup> The electron entry/exit site is the “distal”  $[Fe_4S_4]$  cluster which sits at the end of a chain of three iron–sulfur clusters that span the small (approximately 30 kDa) protein subunit and transfer electrons between the surface of the protein and the bimetallic NiFe  $H_2$ -activating site that is buried in the large (approximately 60 kDa) protein subunit (Figure 1a).<sup>7–12</sup> Soluble and membrane-bound  $O_2$ -sensitive [NiFe]-hydrogenases have this same overall structure;<sup>13–16</sup> in particular, the NiFe centers are identical, and the surrounding architecture is remarkably

Received: April 10, 2017

Published: July 12, 2017

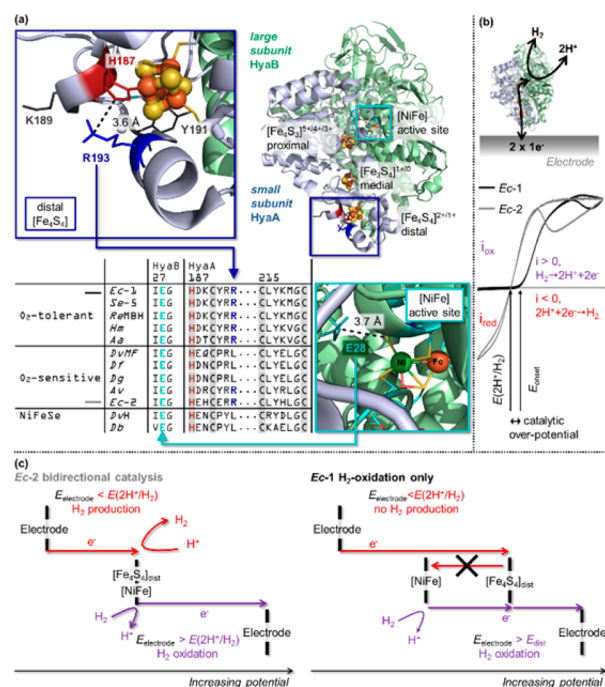


**Figure 1.** (a) *E. coli* hydrogenase-1 structure (PDB 5A4I) with detail of position of HyaB-E28 relative to active site and HyaA-H187, HyaA-R193, HyaA-K189, and HyaA-Y191 relative to the distal cluster. The sequence alignment (*E. coli* Hyd-1 numbering) highlights the conserved nature of E28 in the HyaB protein in *E. coli* Hyd-1 (*Ec-1*), *Salmonella enterica* Hyd-5 (*Se-5*), *Ralstonia eutropha* MBH (*ReMBH*), *Hydrogenovibrio marinus* (*Hm*), *Aquifex aeolicus* (*Aa*), *Desulfovibrio vulgaris* Miyazaki F (*DvMF*), *Desulfovibrio fructosovorans* (*Df*), *Desulfovibrio gigas* (*Dg*), *Allochrochromatium vinosum* (*Av*), *E. coli* Hyd-2 (*Ec-2*), *Desulfovibrio vulgaris* Hildenborough (*DvH*), and *Desulfohalobium baculatum* (*Db*) NiFe or NiFeSe hydrogenases. Also indicated are the distal cluster ligands (gray shading), with dark red text highlighting HyaA-H187 and dark blue text highlighting HyaA-R193. (b) Cartoon depiction of enzyme on electrode and resultant comparative direct current voltammogram traces for either an O<sub>2</sub>-tolerant hydrogenase (*Ec-1*) or an O<sub>2</sub>-sensitive hydrogenase (*Ec-2*) at pH > 5 and under a H<sub>2</sub> atmosphere. The difference in catalytic bias is quantified by the ratio of oxidation current,  $i_{ox}$ , to reduction current,  $i_{red}$ . The onset potential of H<sub>2</sub> oxidation catalysis,  $E_{onset}$ , coincides with the reduction potential for the proton/H<sub>2</sub> couple ( $E(2H^+/H_2)$ ) for an O<sub>2</sub>-sensitive hydrogenase, but there is an overpotential requirement for O<sub>2</sub>-tolerant hydrogenases. (c) Pictorial representation of how simple thermodynamic considerations suggest that unidirectional H<sub>2</sub> oxidation-only catalysis results when  $E_{dist} \gg E(2H^+/H_2)$ . Thermodynamically spontaneous electron transfer can proceed only from left to right; thus electrons can be pushed into the enzyme when  $E_{electrode} < E_{dist}$  or pulled out of the enzyme when  $E_{dist} < E_{electrode}$ . (Left) When  $E_{dist} = E(2H^+/H_2)$ , this results in bidirectional catalysis. (Right) When  $E_{dist} \gg E(2H^+/H_2)$ , H<sub>2</sub> production is prevented by the non-spontaneous movement of electrons from the distal cluster to the active site.

similar. A fully conserved large subunit Glu is found close to the NiFe center in all structures (Figure 1a), and replacement with a nonacidic residue disables catalysis in a number of [NiFe]-hydrogenases,<sup>17–19</sup> suggesting a highly conserved proton transfer relay and mechanism for active site chemistry. Therefore, the NiFe site is unlikely to be the control center for differences in the H<sub>2</sub> reactivity of O<sub>2</sub>-tolerant and O<sub>2</sub>-sensitive [NiFe]-hydrogenases, in contrast with classical models

of enzyme catalysis, which ascribe substrate reactivity and energetics solely to the local environment of the active site.

A unique [Fe<sub>4</sub>S<sub>3</sub>] proximal cluster is required for O<sub>2</sub> tolerance in MBHs,<sup>8–12,20,21</sup> and along with the [Fe<sub>3</sub>S<sub>4</sub>] medial cluster,<sup>22</sup> these centers provide electrons for the reduction of inhibitory O<sub>2</sub> to water at the NiFe site, indicating that iron sulfur cluster chemistry can control active site reactivity. However, in variants with diminished O<sub>2</sub> tolerance due to proximal and medial cluster ligand changes, there is no change in the catalytic reversibility of the enzyme.<sup>12,20–22</sup> Instead, an electrocatalytic model by Hexter et al. proposes that both the catalytic bias and overpotential of multicenter redox enzymes are controlled by the redox potential of the electron entry/exit site, the distal cluster in [NiFe]-hydrogenases.<sup>5,23</sup> Decoding to what extent the redox potential of one electron transfer center can control catalytic reversibility and efficiency is important because hydrogenases are just one example of a large class of electron-relay-containing “wired” metalloenzymes that redox-activate notoriously stable small molecules such as N<sub>2</sub>, H<sub>2</sub>O, and CO<sub>2</sub>.

The tantalizingly simple conclusion of the Hexter model is that complete catalytic reversibility is predicted when the potential of the distal cluster [Fe<sub>4</sub>S<sub>4</sub>]<sup>2+/1+</sup> redox transition,  $E_{dist}$ , matches that of the substrate product couple,  $E(2H^+/H_2)$ .<sup>5,23</sup> Conversely, a mismatch in potentials results in an overpotential and a concurrent catalytic bias.<sup>5,23</sup> In the case of a substantial potential difference the distal cluster essentially acts as an electronic diode, enforcing unidirectional electron flow.<sup>5,23</sup> This is most readily illustrated by a horizontal potential scale diagram, as shown in Figure 1c. Rapid, thermodynamically favorable electron transfer occurs when the reduction potential of the electron donor is more negative than that of the electron acceptor. Thus, it is predicted that the essentially unidirectional, H<sub>2</sub>-oxidizing-only catalysis of O<sub>2</sub>-tolerant MBHs at pH > 5 arises because  $E_{dist} > E(2H^+/H_2)$  over this pH range. The enhanced catalytic reversibility of *E. coli* Hyd-1 at pH < 5 is interpreted as evidence that the potentials of  $E_{dist}$  and  $E(2H^+/H_2)$  converge at low pH.<sup>24</sup> Equally, a catalytic bias toward reduction catalysis (H<sub>2</sub> production) and an overpotential requirement for this activity would be attributed to  $E_{dist} < E(2H^+/H_2)$ .<sup>5,23</sup> In contrast, on the basis of their more complex electrocatalytic model of hydrogenase activity, Léger and co-workers suggest that  $E_{dist}$  will only influence the catalytic reversibility, not completely control it, due to the different nature of the rate-limiting steps in H<sub>2</sub> production and oxidation and the effects of intramolecular electron transfer within the enzyme.<sup>25,26</sup> Comparison of the two models is not possible because there is no experimental measurement of  $E_{dist}$  for *E. coli* Hyd-1,<sup>27</sup> and there have been no [NiFe]-hydrogenase distal cluster variants with a retuned  $E_{dist}$ .

There is a wealth of literature describing how retuning the noncovalent interactions of residues in the second coordination sphere of protein electron transfer centers can have a substantial impact on the redox potential.<sup>28,29</sup> In many O<sub>2</sub>-sensitive [NiFe]-hydrogenases, a Leu residue sits at the apex of the helix between the surface of the protein and the distal cluster His ligand (Figure 1a and Supplementary Figure 1).<sup>13–16</sup> In contrast, sequence comparisons and structural analyses reveal that in all O<sub>2</sub>-tolerant hydrogenases<sup>7–12</sup> a conserved Arg occupies this position, and it is close enough to the distal cluster His ligand for a cation- $\pi$  interaction to persist ( $C\zeta$  to  $N\tau$  from 3.3 to 3.7 Å); that is, there should be an electrostatic attraction between the  $\pi$  electron system of His

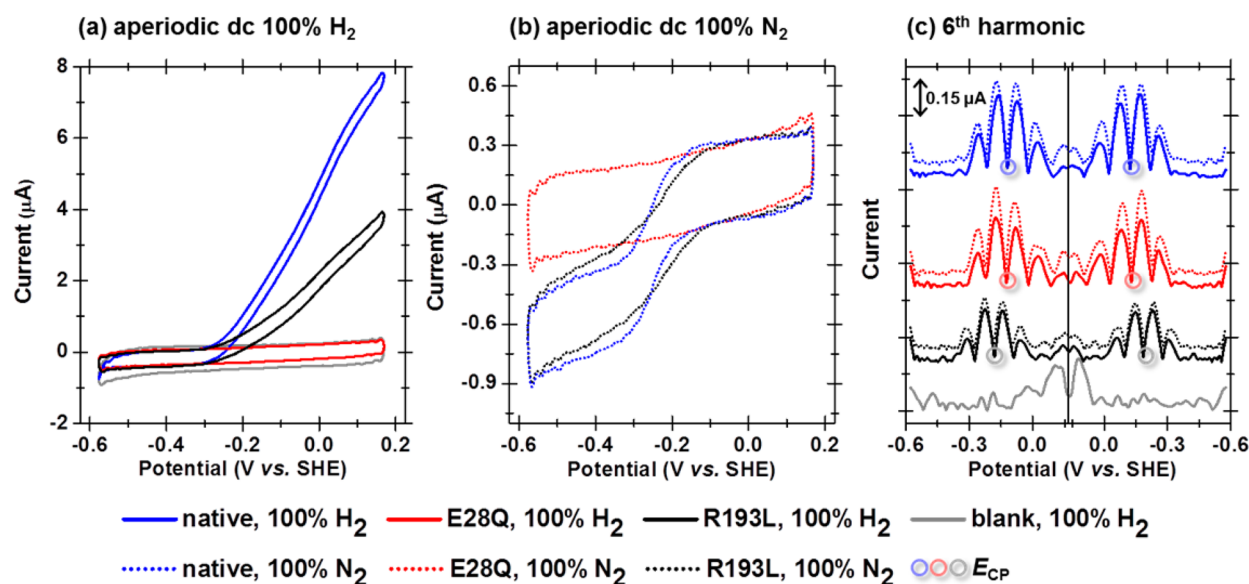


**Figure 2.** FTacV of *E. coli* hydrogenase-1 at frequency = 144 Hz, amplitude = 150 mV, and scan rate = 27.94 mV s<sup>-1</sup>. (a and b) Aperiodic dc component of forward and reverse scans shown as cyclic voltammograms. (c) Sixth-harmonic components of forward and reverse scan. Data sets are offset for clarity, and color code is as indicated, where “blank” refers to an enzyme-free control experiment. Other experimental conditions: pH 4.0, 2000 rpm, 25 °C.

and the positively charged Arg side chain (Figure 1a and Supplementary Figure 2).<sup>30,31</sup> Such interactions have recently been identified as playing a vital role in tuning protein redox chemistry involving Trp residues,<sup>32–35</sup> and we have explored how an *E. coli* Hyd-1 small subunit Arg-193 to Leu amino acid exchange (HyaA-R193L) impacts  $E_{\text{dist}}$  and what the associated catalytic changes are. First coordination sphere ligands are not investigated, as the only previous study on distal cluster variants of a [NiFe]-hydrogenase showed that in the O<sub>2</sub>-sensitive *Desulfovibrio fructosovorans* enzyme changing the Fe-ligating His residue to a Gly or Cys had a strikingly deleterious effect on catalysis (H<sub>2</sub> oxidation activity decreased by at least 97%).<sup>36</sup> Recent density functional theory calculations suggest that this is because electrons pass between the outer surface of the protein and the distal cluster via a precise molecular route that terminates at the His ligand (Supplementary Figure 1).<sup>37,38</sup> Variants HyaA-K189N and HyaA-Y191E, which mimic differences in this surface-to-histidine route in O<sub>2</sub>-tolerant and O<sub>2</sub>-sensitive [NiFe]-hydrogenases (Figure 1), are generated to investigate the role of residues along this route in tuning  $E_{\text{dist}}$ .

EPR measurements do not provide a measure of  $E_{\text{dist}}$  for the genetically tractable enzyme *E. coli* Hyd-1 because the distal center is EPR-silent or -invisible in the oxidized [Fe<sub>4</sub>S<sub>4</sub>]<sup>2+</sup> and reduced [Fe<sub>4</sub>S<sub>4</sub>]<sup>1+</sup> states, respectively.<sup>27</sup> Traditional direct-current voltammetry measurements cannot be used to probe  $E_{\text{dist}}$  because such experiments require noncatalytic conditions,<sup>39</sup> but protons cannot be excluded from aqueous solutions. Although CO is a competitive inhibitor of *Ec* Hyd-1, causing partial inhibition,<sup>4</sup> under an atmosphere of 100% CO the catalytic activity of an O<sub>2</sub>-tolerant hydrogenase cannot be fully inhibited,<sup>40,41</sup> and the enzyme generates enough H<sub>2</sub> to yield a measurable oxidation current. Computational modeling of the protein structure cannot provide a value for  $E_{\text{dist}}$  via direct calculation because the assignment of the electronic levels in iron sulfur clusters is extremely challenging, and such estimates are normally calibrated against unambiguous experimental data.<sup>42</sup> Therefore, in order to provide the first measure of  $E_{\text{dist}}$  we use large-amplitude Fourier-transformed

alternating current voltammetry<sup>43</sup> (FTacV) to probe a hydrogenase for the first time.

In FTacV a large-amplitude sine wave of frequency  $f$  is applied to a voltage sweep and the measured current output is Fourier transformed into the frequency domain to give an aperiodic direct current (dc) component and harmonic signals at multiples of the input frequency ( $f$ ,  $2f$ , etc.). Individual harmonics are band selected and inverse Fourier transformed back to the time domain.<sup>43–45</sup> This is advantageous because in one experiment an FTacV measurement of a redox enzyme and substrate can simultaneously quantify (i) the catalytic current (via the aperiodic dc component) and (ii) noncatalytic, reversible electron transfer processes, such as the distal cluster redox transition [Fe<sub>4</sub>S<sub>4</sub>]<sup>2+/1+</sup>, via the capacitance-free high harmonic current.<sup>45</sup> Thus, unlike traditional voltammetry techniques, in FTacV catalytic current does not mask noncatalytic current, and we describe how this allows us to quantify turnover rates. Complementary EPR experiments probe the redox chemistry of iron–sulfur sites not interrogated via FTacV. We detail the mechanism of how the single HyaA-R193L amino acid exchange enhances bias toward H<sub>2</sub> production and reduces the H<sub>2</sub> oxidation overpotential for an O<sub>2</sub>-tolerant [NiFe]-hydrogenase and show that the variant enzyme retains catalytic activity in the presence of O<sub>2</sub> with slightly diminished tolerance.

## RESULTS

**Separate Resolution of Hydrogenase Catalytic and Noncatalytic Processes by FTacV.** The aperiodic dc and sixth harmonic ac components of high-frequency (144 Hz) and large-amplitude (150 mV) FTacV conducted on as-isolated *E. coli* Hyd-1 adsorbed on a graphite electrode are shown in Figure 2, along with enzyme-free “blank” control data. For native enzyme, the aperiodic dc component is analogous to previous direct current voltammetry (dcV) studies; thus at pH 4.0 negative current corresponding to H<sub>2</sub> production (H<sup>+</sup> reduction) catalysis is detectable under 100% N<sub>2</sub>, but under 100% H<sub>2</sub> only positive current from H<sub>2</sub> oxidation catalysis is

measured.<sup>2</sup> The higher order harmonic signals from the same experiments (displayed as current magnitude plots for the sixth harmonic in Figure 2) are insensitive to the presence of H<sub>2</sub>, indicating that the FTacV technique has enabled the simultaneous and separate measurement of noncatalytic electron transfer in the high harmonics and catalytic current in the aperiodic dc component. For clarity, only the sixth harmonic is depicted in Figure 2, but harmonics 4–7 all provide a background-free measurement of noncatalytic enzyme redox chemistry, Supplementary Figure 3. FTacV conducted at higher pH shows a negative shift in the potential at which a signal is detected in the high-order harmonics and the expected drop in H<sub>2</sub> production current in the aperiodic dc component (Supplementary Figure 4). The amplitude of the sine wave utilized in FTacV affects the apparent onset potential of catalysis in the aperiodic dc component<sup>46</sup> (Supplementary Figure 5), so catalytic overpotential values are assessed in separate dcV experiments described later.

To experimentally corroborate the separate resolution of catalytic and noncatalytic redox processes in 144 Hz FTacV of as-isolated native Hyd-1, a catalytically disabled HyaB-E28Q variant was generated, with the fully conserved proton transfer residue close to the NiFe center (Figure 1) replaced by a nonacidic residue, as first described for *D. fructosovorans* [NiFe]-hydrogenase.<sup>19</sup> The structural integrity of the medial and proximal clusters of HyaB-E28Q was confirmed by EPR measurements (Supplementary Figures 6 and 7), and the catalytic inactivity was established via H<sub>2</sub> oxidation dye assays (Supplementary Figure 8). The aperiodic dc component of 144 Hz FTacV of as-isolated HyaB-E28Q further validates the catalytic inactivity, since there is no discernible H<sub>2</sub> production current under 100% N<sub>2</sub> or oxidation current under 100% H<sub>2</sub>, at pH 4.0 (Figure 2) or higher pH (Supplementary Figure 9). In contrast, the sixth harmonic of 144 Hz FTacV measurements of HyaB-E28Q and native Hyd-1 are almost identical under both 100% N<sub>2</sub> and H<sub>2</sub> (Figure 2 and Supplementary Figure 9), confirming that such high-frequency harmonics provide a measure of purely noncatalytic hydrogenase electron transfer current.

Lower frequency (9 Hz) FTacV measurements of native enzyme do not provide this full separation of catalytic and noncatalytic current. The sixth harmonic of an 8.98 Hz FTacV measurement of native Hyd-1 is sensitive to H<sub>2</sub> (Supplementary Figure 10) and no longer matches that of the inactive HyaB-E28Q (Supplementary Figure 11), indicating a catalytic component to the high harmonic current.<sup>46</sup> Theoretical simulations have previously predicted that for a sufficiently rapid surface-confined catalytic process FTacV will be unable to deconvolute current contributions from reversible electron transfer and substrate turnover.<sup>46</sup> To ensure that our maximum experimental frequency of 144 Hz is always fast enough to generate catalysis-free high harmonic current, as-isolated rather than fully activated Hyd-1 is used for all electrochemical experiments in this study. The catalytic current is lower for as-isolated Hyd-1 because following aerobic purification a proportion of the hydrogenase molecules contain catalytically inactivated Ni sites, which recover activity only upon prolonged (>12 h) exposure to H<sub>2</sub> (Supplementary Figure 8).<sup>4,20,22</sup>

**Assignment of the High-Order Harmonic Signal to Distal Cluster Redox Chemistry.** An automated parameter optimization procedure can be used to determine the values that give the best fit between a model redox reaction and high harmonic FTacV data measured at a low frequency.<sup>44</sup> The 8.88

Hz FTacV measurements of HyaB-E28Q are uncomplicated by any catalytic reactions and were therefore simulated using such a protocol, resulting in a good fit between the experimental data and a model reversible one-electron redox reaction. This yields a measure of the total amount of protein on the electrode,  $M = 0.195$  pmol, and making the usual allowances for a geometric surface area of  $0.03 \text{ cm}^2$  yields a coverage of  $6.5 \text{ pmol cm}^{-2}$ , entirely consistent with the  $3\text{--}12 \text{ pmol cm}^{-2}$  range of coverages observed in the electrochemical study of *Allochromatium vinosum* O<sub>2</sub>-sensitive [NiFe]-hydrogenase by Pershad et al.<sup>39</sup>

Since this is a surface-confined process, we have simulated the problem without including any terms for electrode rotation. Full reversibility is achieved in the model by setting  $k^0$  sufficiently high; in this case we fix  $k^0$  at  $10^4 \text{ s}^{-1}$  (which is equivalent to using the Nernst equation at this low frequency). In this low-frequency regime it would not be possible to detect the distribution in  $k^0$  values, which is predicted by previous models of hydrogenase catalytic wave shapes.<sup>5,23,25,26,47</sup> In studies of single molecules of the copper metalloprotein azurin, a Gaussian distribution of  $E^0$  values has been experimentally observed,<sup>48–51</sup> and we find that incorporation of such thermodynamic distribution is necessary to yield the good fit shown in Figure 3 between the simulation and experimental data (see Supplementary Figure 12). The best fit potential values are average  $E_{\text{rev}} = -123 \text{ mV}$ , and standard deviation =  $31 \text{ mV}$ .

Except for a scalar increase in magnitude, FTacV measurements of HyaB-E28Q at frequencies greater than 8.88 Hz yield sixth-harmonic signals with a very similar current response, indicating that the same redox process is under interrogation (Supplementary Figure 13). The center point potential of the 144 Hz high harmonic signals,  $E_{\text{CP}}$  (the potential of the minimum and maximum current in the center of the even and odd harmonic signals, respectively), corresponds to the simulation-derived average redox potential  $E_{\text{rev}}$  (Figures 2 and 3). Therefore,  $E_{\text{CP}}$ , derived from simple inspection of the 144 Hz FTacV data, is used as a measure of the midpoint potential of the one-electron transfer redox reaction ascribed as giving rise to the noncatalytic current. Since the 144 Hz FTacV high harmonics of native Hyd-1 and HyaB-E28Q are almost identical (Figure 2), the same  $E_{\text{CP}}$  analysis is applied to high-frequency measurements of native Hyd-1 (Supplementary Figure 3). Between pH 3 and 7 the  $E_{\text{CP}}$  of native Hyd-1 and HyaB-E28Q remains essentially indistinguishable, both decreasing as a function of pH with a gradient of  $-18 \text{ mV pH}^{-1}$  (Supplementary Figure 14 and Supplementary Table 1).

Since the 144 Hz FTacV high-harmonic signal of as-isolated native Hyd-1 is insensitive to H<sub>2</sub> and carbon monoxide, an inhibitor that is known to bind at the active site of [NiFe] hydrogenases<sup>1,4</sup> (Supplementary Figure 15), it is unlikely that this current arises from Ni-based redox chemistry. Comparison of  $E_{\text{CP}}$  values with the published potentials of *E. coli* Hyd-1 active site Ni redox transitions<sup>22,52,53</sup> validates this assignment, indicating that the noncatalytic FTacV current must instead arise from iron–sulfur cluster chemistry (Supplementary Table 2 and associated text).

For native Hyd-1 at pH 7.0 the EPR-titration-determined midpoint potentials of the proximal and medial iron–sulfur cluster redox transitions are positive (Supplementary Figure 16 and Supplementary Table 3), while  $E_{\text{CP}} = -176 \pm 3 \text{ mV}$  (Supplementary Table 1). This suggests that it is the EPR-invisible<sup>27</sup> distal cluster redox transition,  $[\text{Fe}_4\text{S}_4]^{2+/1+}$ , under interrogation in the 144 Hz FTacV high harmonics. We cannot

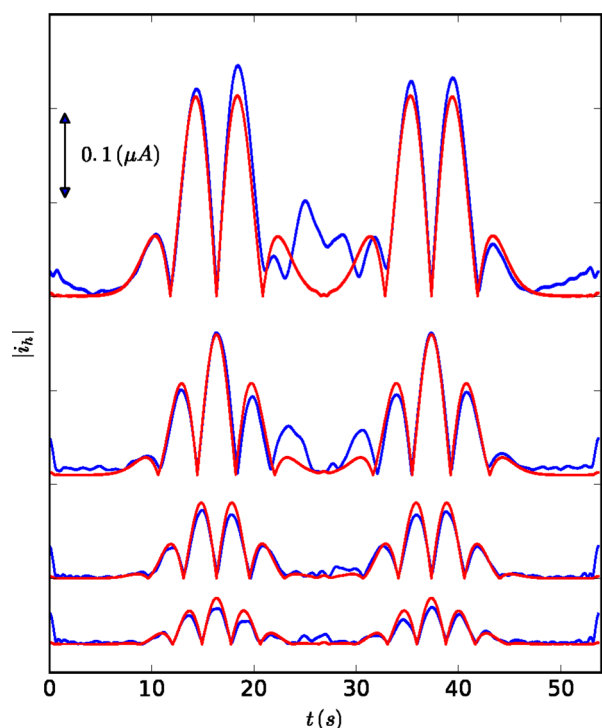


**Figure 3.** Simulation of HyaAB-E28Q FTacV. Overlay of the absolute current magnitudes of the 4th (top) to 7th (bottom) harmonic components of 8.88 Hz FTacV experimental measurement of HyaB-E28Q (blue) and parameter-optimized reversible one-electron reaction simulation (red), as detailed in the text. Each plot was obtained by (i) filtering out the positive frequencies of each harmonic in the frequency domain, (ii) frequency-shifting these down to a center frequency of zero, and then (iii) taking the inverse Fourier transform. Other experimental conditions: amplitude = 150 mV, scan rate = 27.94 mV s<sup>-1</sup>, pH 4.0, 100% H<sub>2</sub> atmosphere, 2000 rpm, 25 °C, uncompensated resistance ( $R_u$ ) = 20 Ω. Simulation parameters: phase = -0.0327, average  $E_{rev}$  = -0.123 V with std dev = 0.031 V,  $\Gamma$  = 6.5 pmol cm<sup>-2</sup>.

measure across a wider potential window in an attempt to also observe current from the medial and proximal cluster redox transitions because the graphite electrode surface ceases to be nonreactive, with faradaic responses attributed to quinone

reactivity<sup>54</sup> observed in enzyme-free “blank” high harmonic FTacV measurements (Supplementary Figure 17).

A HyaA-R193L variant was designed to disrupt the putative cation- $\pi$  interaction between Arg-193 and the distal cluster His-ligand of *E. coli* Hyd-1 (Figure 1). The 144 Hz FTacV sixth harmonic of HyaA-R193L is insensitive to H<sub>2</sub> and retains the same shape as native Hyd-1 and HyaB-E28Q (Figure 2 and Supplementary Figure 9), suggesting that a one-electron noncatalytic redox reaction is again measured. However, because of the amino acid exchange, across the pH range 3 to 7 the  $E_{CP}$  shifts by approximately -60 mV relative to native Hyd-1 and HyaB-E28Q (Figure 2 and Supplementary Figures 9 and 14). We interpret this as further evidence that the distal cluster  $[\text{Fe}_4\text{S}_4]^{2+/1+}$  transition is under interrogation, and from this point it is assumed that  $E_{CP}$  values are equivalent to  $E_{dist}$ .

**Relating the Distal Cluster Potential to Catalytic Bias and Overpotential.** Having determined that FTacV permits measurement of  $E_{dist}$  and generated a variant with a retuned  $E_{dist}$ , we now compare the catalytic activity of native Hyd-1 and HyaA-R193L to explore the role of the distal cluster in controlling catalytic bias and overpotential in [NiFe]-hydrogenases. A visual inspection of the aperiodic dc component of pH 4.0 144 Hz FTacV (Figure 2) suggests that HyaA-R193L is less biased toward H<sub>2</sub> oxidation than native Hyd-1. Under 100% N<sub>2</sub> the maximum H<sub>2</sub> production currents of native Hyd-1 and HyaA-R193L are similar, but under 100% H<sub>2</sub> the H<sub>2</sub> oxidation current of HyaA-R193L is significantly lower. A quantitative measure of the changes in turnover rates that led to a change in catalytic bias can only be obtained via knowledge of the number of active moles of enzyme on the electrode,  $M_{active}$ . This parameter is normally unmeasurable in the dcV of O<sub>2</sub>-tolerant MBHs.<sup>2</sup> FTacV permits estimation of  $M_{active}$ , and we do so based on  $i_{max}^{144\text{ Hz}}_{6th}$ , the maximum current magnitude of the 144 Hz FTacV sixth harmonic. Simulation of 8.88 Hz FTacV of HyaB-E28Q quantified the total amount of hydrogenase on the electrode as  $M = 0.195$  pmol (Figure 3) and when this same protein film was interrogated at 144 Hz,  $i_{max}^{144\text{ Hz}}_{6th} = 0.285$  μA (Supplementary Figure 13). For a reversible one-electron reaction the harmonic current magnitude scales linearly with  $M$ ,<sup>46</sup> so it is extrapolated that  $M(\text{mol}) \approx 6.8 \times 10^{-7} \times i_{max}^{144\text{ Hz}}_{6th}$  for all variants. Since as-isolated enzyme is interrogated, some hydrogenase molecules are inactive and  $M \neq M_{active}$ . Dye assay

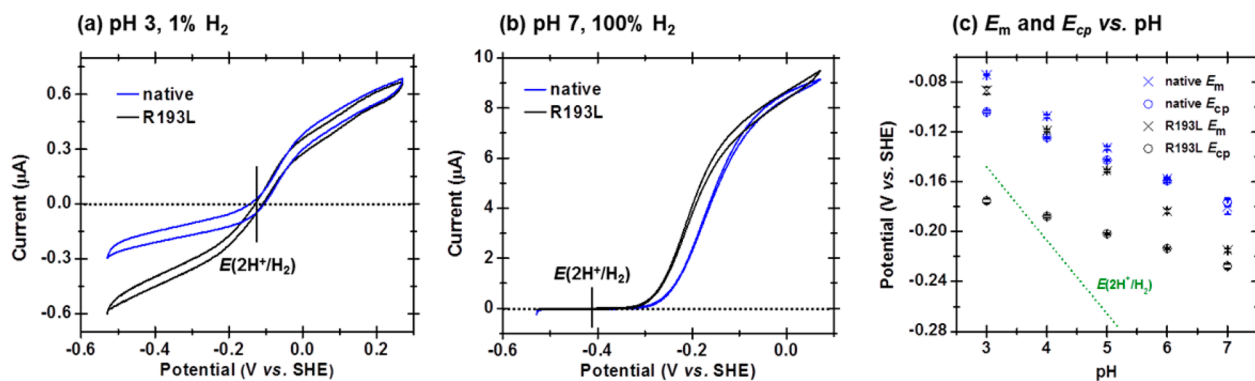


**Figure 4.** Comparison of the catalytic bias and overpotential requirement of native Hyd-1 and HyaA-R193L. (a) dcV experiment to emphasize increased bias toward H<sub>2</sub> production of *E. coli* hydrogenase-1 HyaA-R193L variant relative to native enzyme. (b) dcV experiment to highlight the decreased catalytic overpotential of HyaA-R193L relative to native Hyd-1. Other experimental conditions: scan rate = 5 mV s<sup>-1</sup>, 25 °C, 5000 rpm, pH and gas atmosphere as indicated. (c) pH dependence of the H<sub>2</sub>-independent 144 Hz FTacV determined sixth-harmonic  $E_{CP}$ ,  $E_m$  from dcV experiments conducted in 10% H<sub>2</sub>, and the Nernstian-determined  $E(2\text{H}^+/\text{H}_2)$  value at 10% H<sub>2</sub>. Error bars show standard error of at least three repeats.

data indicate that following overnight incubation in  $H_2$ , activity increases by a scalar factor of approximately 3 for both native Hyd-1 and HyaA-R193L, and so it is estimated that  $M_{\text{active}} \approx \frac{M}{3}$  (Supplementary Figure 8).

The turnover rate,  $k_{H_2}$ , can thus be calculated from a single 144 Hz FTacV measurement (Figure 2) using the equation  $k_{H_2} = \frac{i_{\text{cat}}}{2M_{\text{active}}F}$ , where  $F$  is the Faraday constant.<sup>39</sup> Averaging the catalytic current measured at a certain potential in the forward and back sweep of the aperiodic dc component yields  $i_{\text{cat}}$  while  $M_{\text{active}}$  is estimated from the sixth harmonic. Analysis of repeat experiments conducted at pH 4.0, 25 °C, and under 100%  $H_2$  quantifies  $H_2$  oxidation turnover rates at +150 mV of 510, 790, and 750  $s^{-1}$  for native Hyd-1 and 390, 320, and 190  $s^{-1}$  for HyaA-R193L. Similarly,  $H_2$  production rates at −550 mV, pH 4.0, 25 °C, and under 100%  $N_2$  are measured as 45, 51, and 48  $s^{-1}$  for native Hyd-1 and 75, 60, and 57  $s^{-1}$  for HyaA-R193L. As has been previously noted for hydrogenases, the electrocatalytic turnover rates exceed those from the solution assays, suggesting that diffusion may play a limiting role when the enzyme is not directly attached to its electron exchange partner.<sup>40</sup> There is significant variability in the absolute turnover rates extracted, which can be attributed to error in our quantification of  $M_{\text{active}}$ , but the analysis suggests that HyaA-R193L is more biased toward  $H_2$  production catalysis than native enzyme due to a decrease in  $H_2$  oxidation rate and a possible increase in  $H_2$  production rate.

Catalytic onset potentials are quantified via dcV experiments (Figure 4). At pH 3.0 and under 1%  $H_2$  both native Hyd-1 and HyaA-R193L have zero overpotential requirement, since both oxidative and reductive catalysis commence at the potential of  $E(2H^+/H_2)$  (Figure 4a). Since the catalysis is reversible, an absolute measure of catalytic bias can be obtained. The ratios of the  $H_2$  oxidation current at +0.13 V and  $H^+$  reduction current at −0.37 V (both taken from the average of the forward and back sweep) are  $3.2 \pm 0.2$  for native Hyd-1 and  $1.1 \pm 0.2$  for HyaA-R193L ( $\pm$  indicates standard error of three repeats for different enzyme “films”). The change in bias cannot be attributed to changes in the Michaelis constant ( $K_M$ ) or the inhibition constant ( $K_I$ ) for  $H_2$  (Supplementary Figure 18 and Supplementary Table 4), suggesting that the lowering of  $E_{\text{dist}}$  has either directly or indirectly led to a concomitant shift in catalytic bias toward  $H_2$  production in HyaA-R193L.

At pH 7.0 and under 100%  $H_2$  both native Hyd-1 and HyaA-R193L are unidirectional,  $H_2$  oxidation-only catalysts (Figure 4b). Both enzymes have an overpotential requirement for  $H_2$  oxidation, since catalysis does not commence until a potential significantly higher than  $E(2H^+/H_2)$ . The onset of catalysis is clearly shifted to lower potential for HyaA-R193L, making it a more thermodynamically efficient  $H_2$  oxidation catalyst than native Hyd-1 and confirming a relationship between  $E_{\text{dist}}$  and catalytic overpotential.

To quantify the impact of pH on the onset potential of  $H_2$  oxidation catalysis, 10%  $H_2$  dcV experiments in which native Hyd-1 and variant HyaA-R193L had similar maximum oxidative currents were analyzed. The onset potential is compared by characterizing a catalytic potential  $E_m$ , the potential of the maxima in a first derivative  $di_{\text{av}}/dE$  vs  $E$  plot, where  $i_{\text{av}}$  is the average of the forward and back current. Defining this parameter also facilitates comparison between  $E_{\text{dist}}$  and the potential of  $H_2$  oxidation catalysis. As shown in Figure 4c, at pH 3.0 both native Hyd-1 and HyaA-R193L are thermodynamically

optimized catalysts with similar  $E_m$  values close to  $E(2H^+/H_2)$ . Thus, the difference in the  $E_{\text{dist}}$  values does not apparently impact the thermodynamic efficiency of catalysis under these conditions. However, as the pH increases from 3.0 to 7.0, the  $E_m$  of HyaA-R193L becomes increasingly more negative than that of native Hyd-1, suggesting that the difference in  $E_{\text{dist}}$  values has a significant impact on the overpotential requirement for  $H_2$  oxidation under conditions of high pH.

**Further Impact of the HyaA-R193L Amino Acid Exchange.** Relative to native enzyme, the catalytic profile of HyaA-R193L has been tuned toward that of an  $O_2$ -sensitive [NiFe]-hydrogenase, with enhanced bias toward  $H_2$  production and decreased  $H_2$  oxidation overpotential. To examine if  $O_2$  tolerance has been maintained following this amino acid exchange, inhibition of  $H_2$  oxidation by 3%  $O_2$  in 3%  $H_2$  was quantified using chronoamperometry at −0.029 V, pH 6.0, and 25 °C (Supplementary Figure 19). HyaA-R193L is  $O_2$ -tolerant, but this tolerance is slightly impaired relative to native Hyd-1; for HyaA-R193L approximately 60% of initial oxidation activity is sustained in 3%  $O_2$ /3%  $H_2$  and approximately 85% of original activity is rapidly recovered when the  $O_2$  is removed; for native Hyd-1 approximately 75% activity is sustained and approximately 95% is recovered.

There is also a small difference between HyaA-R193L and native Hyd-1 in the reversible anaerobic formation of the Ni–B (Ni(III)–OH) inactivated state at positive potential. Formation of the Ni–B state was achieved via a 1000 s hold at +0.451 V, and reactivation was driven by a 0.25 mV  $s^{-1}$  linear sweep to low potential, under 10%  $H_2$  at 25 °C (Supplementary Figure 20). A qualitative measure of the thermodynamics and kinetics of Ni–B reactivation is given by  $E_{\text{switch}}$ , the potential at which the recovering catalytic current increases most rapidly (potential of the first derivative minima) in the sweep to low potential.<sup>55</sup> HyaA-R193L has a marginally (<10 mV) more negative  $E_{\text{switch}}$  than native Hyd-1 across the pH range 4.0 to 8.0 (Supplementary Figure 20), indicating slightly slower activation kinetics and/or a slightly more negative Ni–B reduction potential.<sup>55</sup> This difference in  $E_{\text{switch}}$  is less than the 15 to 30 mV difference in  $E_m$  (potential of the first derivative maxima) observed in the same experiments (Supplementary Figure 20).

Such changes in anaerobic inactivation and  $O_2$  tolerance of *E. coli* Hyd-1 have previously been related to modifications of the proximal and medial clusters, rather than changes at the distal cluster.<sup>20,22</sup> EPR titrations at pH 7.0 reveal that the midpoint potentials associated with the medial cluster  $[3Fe_4S_3]^{1+/0}$  and proximal cluster  $[Fe_4S_3]^{5+/4+}$  redox transitions are more negative in HyaA-R193L than native Hyd-1, decreased by approximately 0.11 and 0.04 V, respectively (Table 1 and Supplementary Figures 21 and 22). Thus, retuning the distal cluster potential also impacts the medial and proximal cluster potentials, indicating a highly convoluted structure–function relationship.

**Table 1. EPR-Determined Iron Sulfur Cluster Midpoint Potentials at pH 7.0**

redox transition	native Hyd-1 <sup>a</sup>	HyaA-R193L <sup>a</sup>
proximal $[Fe_4S_3]^{5+/4+}$	211 mV ( $\pm 15$ )	170 mV ( $\pm 15$ )
medial $[Fe_3S_4]^{1+/0}$	212 mV ( $\pm 30$ )	103 mV ( $\pm 30$ )
proximal $[Fe_4S_3]^{4+/3+}$	4 mV ( $\pm 15$ )	−4 mV ( $\pm 15$ )

<sup>a</sup>Errors were estimated by using signal intensities at different field positions ( $g$  values) arising from the same species.

**Distal Cluster Variants HyaA-K189N, HyaA-Y191E, and HyaA-R193E.** The variants HyaA-K189N and HyaA-Y191E have the same distal cluster redox potential as native Hyd-1, as quantified by  $E_{CP}$ , despite these residues also being in the vicinity of the distal cluster and the amino acid exchanges being inspired by differences between  $O_2$ -tolerant MBHs and  $O_2$ -sensitive [NiFe]-hydrogenases (Figure 1 and Supplementary Figures 23 and 24). The catalytic activity of both variants is also unchanged compared to native enzyme (Supplementary Figures 25 and 26). Attempts were also made to generate a HyaA-R193E variant, to investigate if a distal cluster with even more negative potential would result from replacing the positively charged Arg residue with a negatively charged Glu. However, growth and protein purification from the relevant *E. coli* mutant did not yield this Hyd-1 variant, suggesting that this amino acid exchange has a deleterious impact on the structural integrity of the enzyme (Supplementary Figure 27).

## DISCUSSION

Using *E. coli* Hyd-1, we prove that the bias and overpotential of the  $2H^+/H_2$  interconversion that takes place at the buried NiFe active site of a hydrogenase can be altered by a single amino acid exchange near the distal cluster electron entry/exit site, approximately 30 Å away. Engineering  $E_{dist}$  to a more negative potential correlated with an enhanced bias toward  $H_2$  production and decreased overpotential for  $H_2$  oxidation, while catalytic activity in the presence of  $O_2$  was maintained but with diminished tolerance. [NiFe]-hydrogenase  $H_2$  production activity is important for developing biological and bioinspired solar  $H_2$  devices.<sup>6,56</sup> Decreasing the overpotential in [NiFe]-hydrogenase  $H_2$  oxidation would also improve the thermodynamic efficiency of fuel cell and NAD(P)H recycling devices which use these enzymes instead of Pt.<sup>3,57</sup> The previously elusive parameter  $E_{dist}$  is measured using high-frequency, high-harmonic FTacV measurements and manipulated via an R193 to L amino acid exchange that is based on the first proposal of a His-mediated cation- $\pi$  interaction tuning the redox chemistry of an FeS cluster.

By utilizing FTacV to interrogate *Ec* Hyd-1 we could work in the frequency domain to analyze our experimental data. This allows us to focus on those parts of the experimental signal that yield a further understanding of electron transfer in/out of the distal cluster, effectively filtering out the catalytic current. We thus derive an FTacV-determined pH 7  $E_{dist}$  value of -176 mV for native *Ec* Hyd-1. When combined with our EPR-measured proximal cluster  $[Fe_4S_3]^{4+/3+}$  pH 7 midpoint potential of 4 mV, this suggests a significant difference in the redox properties of the clusters from the  $O_2$ -tolerant [NiFe]-hydrogenases of *Ec* and *Aa*. This is in line with known apparent magnetic differences between these centers. The 2011 EPR interrogation of *Aa* MBH by Pandelia and co-workers reported signals assigned to two different 4Fe clusters at low potential; the proximal cluster  $[Fe_4S_3]^{4+/3+}$  was assigned a midpoint of +87 mV, and  $E_{dist}$  was measured as -78 mV, both at pH 7.4.<sup>58,59</sup> However, in the 2012 EPR study of *Ec* Hyd-1,<sup>27</sup> spin-counting and pulse EPR measurements on native enzyme and three variants established that the distal cluster in this enzyme has a ground state of  $S > 1/2$ . The *Ec* Hyd-1 EPR-visible signal from a 4Fe cluster at low potential was therefore assigned to the most reduced state of the proximal cluster,<sup>27</sup> as here. The lack of a structure for the *Aa* enzyme presents a significant barrier in unraveling these striking differences in two enzymes that have similar sequences around the distal cluster.

Cation- $\pi$  interactions between a positively charged amino acid side chain and the  $\pi$  system of an aromatic side chain are well documented in structural biology, but much less commonly considered in the tuning of protein redox sites.<sup>30</sup> In all  $O_2$ -tolerant MBH crystal structures an Arg residue points at the distal cluster His ligand with close enough proximity for a cation- $\pi$  interaction to exist.<sup>7-12</sup> Replacement of the positive Arg residue with a neutral Leu, found in many  $O_2$ -sensitive [NiFe]-hydrogenases,<sup>13-16</sup> results in a HyaA-R193L variant with an FTacV-determined  $E_{dist}$  approximately 60 mV more negative than that of native *E. coli* Hyd-1 across the pH range 3.0 to 7.0. Thus, removal of the putative electrostatic cation- $\pi$  interaction has increased the thermodynamic driving force required to reduce the distal cluster. This can be rationalized by considering that the cation- $\pi$  interaction serves to withdraw electron density from the cluster in the native enzyme, stabilizing the reduced state. Therefore, cation- $\pi$  interactions should be considered alongside other electrostatic, hydrogen-bonding, and hydrophobic interactions in the tuning of protein redox site reduction potentials by secondary coordination sphere effects.

As well as changing  $E_{dist}$ , the R to L amino acid exchange also impacted the medial and proximal iron-sulfur cluster potentials. Thus, we cannot deconvolute which aspects of the reactivity of HyaA-R193L are solely attributable to the low value of  $E_{dist}$ , although it is notable that previous changes to the proximal and medial cluster potentials have had no impact on overpotential or catalytic bias.<sup>12,20-22</sup> The fact that the redox potential of one center in an electron transfer relay influences the redox potential of other centers is a well-observed phenomenon that has been reported for other [NiFe]-hydrogenase variants.<sup>19,20,22,27,36</sup> Accounting for this interdependency further complicates attempts to computationally model metalloenzyme chemistry and highlights the need for continuing experimentation.

The notion that the catalytic bias of Hyd-1 could be changed by altering  $E_{dist}$  was inspired by the electrocatalytic model of Hexter et al.<sup>5,23</sup> This simple model predicted a convergence in  $E_{dist}$  and  $E(2H^+/H_2)$  for native Hyd-1 at low pH, and this is proved. However, the model is not entirely validated; at pH 3.0 and 1%  $H_2$  variant HyaA-R193L is equally biased toward  $H_2$  oxidation and production, despite the model predicting more  $H_2$  production activity since  $E_{dist}$  is more negative than  $E(2H^+/H_2)$  (-175 and -118 mV, respectively).<sup>5,23</sup> Thus, although changes to the catalytic bias can be somewhat correlated with changes to the distal cluster potential, further factors must also control this important enzymatic property. This conclusion is supported by previous studies showing that mutation of amino acid residues distant from the distal cluster can alter the catalytic bias of [NiFe]-hydrogenases.<sup>6,60</sup> The simple Hexter model implicitly assumes that the distal cluster controls both oxidative and reductive catalysis, but our pH 4.0 FTacV rates analyses indicate that the HyaA-R193L amino acid exchange results in a much larger decrease in  $H_2$ -oxidation rate than increase in  $H_2$ -production rate.<sup>5,23</sup> Thus, enzyme wiring appears to play a more vital role in controlling  $H_2$  oxidation than  $H_2$  production. This supports the more complex model of [NiFe]-electrocatalysis proposed by Léger et al., who suggest that the rate of  $H_2$  production catalysis is significantly limited by slow  $H_2$  release from the active site.<sup>25,26</sup> Although the simple Hexter model has provided an excellent blueprint for substantially retuning the catalysis of Hyd-1, if the rate of  $H_2$  production is

to be further enhanced, large subunit changes that impact the rate of H<sub>2</sub> release from the active site may be required.

The electrocatalytic models of both Hexter et al.<sup>5,23</sup> and Léger and co-workers<sup>25,26</sup> also predict a relationship between  $E_{\text{dist}}$  and catalytic overpotential that we experimentally validate. At pH 7.0 the difference in the H<sub>2</sub> oxidation  $E_{\text{m}}$  potentials of native Hyd-1 and variant HyaA-R193L can be very closely correlated to the difference in  $E_{\text{dist}}$  values, and HyaA-R193L is a substantially more thermodynamically efficient catalyst (Figure 4). Again, designating  $E_{\text{dist}}$  as the sole variable that controls this aspect of electrocatalysis is shown to be an oversimplification of the Hexter model.<sup>5,23</sup> At pH 3.0 the  $E_{\text{m}}$  values of both native Hyd-1 and HyaA-R193L converge, despite the approximately 60 mV difference in  $E_{\text{dist}}$  values. Thus, the distal cluster potential is not in total control of the catalytic potential at all pH's, in accordance with the electrocatalytic model of Léger and co-workers,<sup>25,26</sup> which predicts that both intramolecular and intermolecular electron transfer control catalysis. However, when the potential difference between the substrate potential and that of the electron entry/exit site in the enzyme is sufficiently large, the redox potential of the outermost electron transfer center apparently controls overpotential and, therefore, offers a single point of focus for catalytic retuning strategies.

Conflicting hydrogenase electrocatalysis models exist because large numbers of parameters are required to describe substrate turnover in such complex enzymes. A significant implication of our work is the fact that we determine a lower limit for  $k^0$ , a key electrocatalytic modeling parameter that has been indirectly derived or fitted in all previous hydrogenase electrocatalytic models.<sup>3,5,23,25,26,47,61</sup> Ongoing work will focus on using FTacV to measure the redox chemistry of the medial and proximal clusters and the distribution in  $k^0$  that is believed to arise from dispersion in the orientation of enzyme of the electrode surface.<sup>47</sup> It is only through quantifying such parameters that it will be possible to unambiguously probe the mechanistic origin of the complex voltammetry of hydrogenases.

Nitrogenase,<sup>62</sup> carbon monoxide dehydrogenase,<sup>63</sup> and Photosystem II<sup>64</sup> enzymes also convert small molecules into their redox-activated and chemically useful counterparts (N<sub>2</sub> to NH<sub>3</sub>, CO<sub>2</sub> to CO, and H<sub>2</sub>O to O<sub>2</sub>, respectively) and contain a relay of redox-active centers that wire the outer surface of the protein to the “buried” active sites. FTacV should be considered a very useful tool for probing such systems and exploring how the electron transfer centers control catalysis in these redox enzymes. Ultimately, the inclusion of a molecular wire may be found to be an important design principle for synthetic multielectron redox catalysts, which typically lack such additional redox centers.

## ■ EXPERIMENTAL SECTION

**Molecular Biology.** All native and variant Hyd-1 enzymes were produced from W3110-derived *E. coli* K-12 strain LAF003 and variant strains. Strain LAF003 has an engineered *hyaA(his<sub>7</sub>)BCDEF* operon to produce “wild-type” *E. coli* hydrogenase-1 with a polyhistidine tag at the C terminus of the small subunit.<sup>60</sup> Five variant strains, carrying chromosomal *hyaB*(E28Q), *hyaA*(R193L), *hyaA*(R193E), *hyaA*(K189N), and *hyaA*(Y191E) mutations, were derived from LAF003 using the “counter-selection BAC modification kit” (Cambio) and the protocol detailed previously.<sup>60</sup> Briefly, the *rpsL*-neo cassette was inserted into an appropriate region of *hyaB* or *hyaA* of strain LAF003 to generate strains HA001 and HA002, respectively. The cassette was swapped out of HA001 by linear DNA (HyaBE28Qds-frag), to give strain HA003 encoding a chromosomal E28Q mutation in *hyaB*. The cassette was swapped out of HA002 by linear DNA to

give strains HA004, HA005, HA011, and HA014 encoding chromosomal mutations R193L, R193E, K189N, or Y191E, respectively, in *hyaA*. All mutations were confirmed by sequencing (GATC Biotech). Details of all strains, oligonucleotide primers, plasmids, and linear DNA used in this study are given in [Supplementary Tables 5–8](#).

**Protein Production and Purification.** All strains were grown and proteins produced using a similar protocol to that detailed previously.<sup>60</sup> Briefly, strains were cultured anaerobically, harvested at stationary phase, lysed by osmotic shock then sonication, and solubilized overnight by addition of 3% TritonX-100. Solubilized protein was purified by adding 50 mM imidazole and loading onto a 5 mL HiTrap Ni affinity column (GE Healthcare) that had been equilibrated in 20 mM Tris, 150 mM NaCl, and 50 mM imidazole, pH 7.3. Protein was eluted from the column using step changes in imidazole, up to a maximum concentration of 1 M, with all other buffer components unchanged. Fractions containing hydrogenase were confirmed by SDS-PAGE, pooled, and then dialyzed in a 20 mM Tris and 150 mM NaCl, pH 7.3, buffer overnight at 4 °C using 6–8 kDa MWCO dialysis tubing (Fisher). Protein was concentrated using a 50 kDa MWCO Vivaspin centrifugal concentrator (GE Healthcare), and purity was confirmed by SDS-PAGE ([Supplementary Figures 28 and 29](#)).

For EPR samples the protein was then dialyzed in 50 mM HEPES, 50 mM dibasic sodium phosphate, 150 mM NaCl, and 30% v/v glycerol, pH 7.0, using a 3.5 kDa MWCO Slide-A-Lyzer cassette (ThermoFisher).

For all assay and electrochemical experiments the protein was further purified by gel filtration on a Superdex 200 10/30 column (GE Healthcare) equilibrated in 20 mM Tris and 150 mM NaCl, pH 7.3. Fractions containing completely pure hydrogenase were confirmed by SDS-PAGE, pooled, and concentrated using a 50 kDa MWCO Vivaspin centrifugal concentrator (GE Healthcare). Final sample purity was confirmed by SDS-PAGE ([Supplementary Figures 28 and 29](#)), and protein concentrations were measured by Bradford assay.

**Protein Film Electrochemistry.** All electrochemical experiments (dcV and FTacV) were performed in an anaerobic glovebox (University of York, Department of Chemistry, Mechanical Workshop). A three-electrode setup of a platinum counter, pyrolytic graphite edge (PGE) working electrode (geometric surface area 0.03 cm<sup>2</sup>) and saturated calomel electrode (SCE) reference electrode was used, with a conversion factor of  $E(\text{V vs SHE}) = E(\text{V vs SCE}) + 0.241$ . All electrodes were contained in a water-jacketed and gastight glass cell containing a mixed buffer of 15 mM each of MES, CHES, HEPES, TAPS, and Na acetate and 2 M NaCl. The temperature was controlled to 25 °C by a water circulator, and the atmosphere regulated by 100 standard cubic centimeters per minute flow of gas (BOC) of a certain composition by mass flow controllers (Sierra Instruments).

To prepare an enzyme film, the PGE surface was abraded with P1200 sandpaper (Norton), and then 0.5  $\mu\text{L}$  of a 0.25–1.5 mg mL<sup>−1</sup> protein applied to the electrode surface for ~30 s, before excess enzyme was removed with a stream of water (Purite, 7.4 M $\Omega$ ·cm). An Origiator rotator (Origalys) was used to rotate the working electrode at 2000–5000 rpm to ensure mass transport of substrate or product was not rate limiting to catalysis. Direct current cyclic voltammetry and chronoamperometry measurements were performed with an Ivium CompactStat potentiostat. All Fourier-transformed ac voltammetry was performed using the custom-made instrumentation described previously.<sup>43</sup> Impedance was measured at potentials devoid of Faradaic current, and a simple RC circuit model was used to calculate the uncompensated resistance value used in simulations.

**Simulations.** Simulations were performed using a protocol based on those previously described in Morris et al.<sup>51</sup> and Adamson et al.<sup>44</sup> We assumed a Langmuir isotherm, and any proton transfer accompanying electron transfer is reversible, with the equilibrium constants associated with protonation incorporated into  $E_{\text{rev}}$ . More details are provided in the [Supporting Information](#).

**EPR.** EPR titrations were performed as detailed previously.<sup>60,65</sup> Briefly, 100–200  $\mu\text{L}$  of enzyme solution in pH 7.0 buffer (above) was transferred to a custom electrochemical cell with a platinum working

electrode and Ag/AgCl reference electrode (3 M KCl, DRIF-2, WPI) inside a Braun UniLab-plus glovebox ( $O_2 < 0.5$  ppm,  $N_2$  atmosphere). The following redox mediators were added to a final concentration of 25  $\mu$ M (native Hyd-1 and HyaB-E28Q) or 40  $\mu$ M (HyaA-R139L): phenazine methosulfate, 1,4-naphthoquinone, methylene blue, indigo trisulfonate, 2-hydroxy-1,4-naphthoquinone, benzyl viologen, and methyl viologen. In addition, 40  $\mu$ M anthraquinone-2-sulfonate was added to the HyaA-R139L sample. Each hydrogenase sample was titrated by the addition of small aliquots of potassium ferricyanide or sodium dithionite until the desired potential was achieved, at which stage 9  $\mu$ L samples were transferred to quartz EPR tubes (1.6 mm outer diameter, Wilmad) and flash frozen in ethanol cooled externally using a dry ice/acetone bath.

EPR measurements were performed on an X/Q-band Bruker Elexsys E580 spectrometer (Bruker BioSpin GmbH, Germany) equipped with a closed-cycle cryostat (Cryogenic Ltd, UK) and an X-band split-ring resonator module with 2 mm sample access (ER 4118X-MS2, Bruker) operated in continuous-wave mode. All measurements were conducted at 20 K with 2 mW power, 100 kHz modulation frequency, and 1.0 mT modulation amplitude. In order to determine reduction potentials of the EPR-visible clusters, signal intensities were monitored as a function of potential ("Nernst plots" in Supplementary Figures 16 and 21). The proximal  $[Fe_4S_3]^{5+/4+}$  signal intensity was plotted using the difference in peak heights at  $g = 1.981$  and 1.970, with the maximum intensity scaled to 1. The  $[Fe_4S_3]^{4+/3+}$  intensities were taken from the height of the EPR signal at  $g = 1.892$ –1.871. The intensity of the medial  $[Fe_3S_4]^{1+}$  cluster EPR signal (that decreased at high potentials due to magnetic coupling with  $[Fe_4S_3]^{5+}$ ) was monitored using  $g = 2.025$ –1.981 (native Hyd-1) or  $g = 2.059$ –2.025 (HyaA-R139L). The reduction potential of the medial cluster  $[Fe_3S_4]^{+/0}$  transition was determined as described in Roessler et al.<sup>27</sup> The double integral of the EPR spectrum from the most oxidized sample was normalized to two spins per enzyme molecule to account for the fully oxidized medial and proximal clusters. The percentage of signal arising from the medial cluster was then determined by subtraction of the percentage of signal arising from the proximal cluster (established from its reduction potential). Signal intensities from the medial  $[3Fe-4S]^+$  signal were then scaled according to the percentage reduction of the cluster.

## ■ ASSOCIATED CONTENT

### Supporting Information

The Supporting Information is available free of charge on the ACS Publications website at DOI: 10.1021/jacs.7b03611.

Additional information (PDF)

## ■ AUTHOR INFORMATION

### Corresponding Author

\*alison.parkin@york.ac.uk

### ORCID

Alison Parkin: 0000-0003-4715-7200

### Present Address

#School of Biomedical Sciences, University of Leeds, LS2 9JT, UK.

### Notes

The authors declare no competing financial interest.

## ■ ACKNOWLEDGMENTS

The research leading to these results has received funding from the Royal Society (International Exchange Grant to H.A., A.M.B., and A.P.); BBSRC (studentship BB/F017316/1 to H.A.); Australian Research Council (Discovery Project DP170101535 to A.M.B., D.J.G., and A.P.); EPSRC ("2020 Science" funded through Cross-Disciplinary Interface Programme EP/I017909/1 to M.R. and D.J.G., studentship EP/

M506394/1 to J.J.W., and First Grant EP/M024393/1 to M.M.R.); Wellcome Trust (Combating Infectious Disease: Computational Approaches in Translational Science (WT095024MA) studentship to L.A.F.); and the University of York (J.W. and A.P.).

## ■ REFERENCES

- (1) Lubitz, W.; Ogata, H.; Rüdiger, O.; Reijerse, E. *Chem. Rev.* **2014**, *114* (8), 4081–4148.
- (2) Flanagan, L. A.; Parkin, A. *Biochem. Soc. Trans.* **2016**, *44* (1), 315–328.
- (3) Armstrong, F. A.; Evans, R. M.; Hexter, S. V.; Murphy, B. J.; Roessler, M. M.; Wulff, P. *Acc. Chem. Res.* **2016**, *49* (5), 884–892.
- (4) Lukey, M. J.; Parkin, A.; Roessler, M. M.; Murphy, B. J.; Harmer, J.; Palmer, T.; Sargent, F.; Armstrong, F. A. *J. Biol. Chem.* **2010**, *285* (6), 3928–3938.
- (5) Hexter, S. V.; Grey, F.; Happe, T.; Climent, V.; Armstrong, F. A. *Proc. Natl. Acad. Sci. U. S. A.* **2012**, *109* (29), 11516–11521.
- (6) Raleiras, P.; Khanna, N.; Miranda, H.; Meszaros, L. S.; Krassen, H.; Ho, F.; Battchikova, N.; Aro, E.-M.; Magnuson, A.; Lindblad, P.; Styring, S. *Energy Environ. Sci.* **2016**, *9* (2), 581–594.
- (7) Evans, R. M.; Brooke, E. J.; Wehlin, S. A. M.; Nomerotskaia, E.; Sargent, F.; Carr, S. B.; Phillips, S. E. V.; Armstrong, F. A. *Nat. Chem. Biol.* **2016**, *12* (1), 46–50.
- (8) Fritsch, J.; Scheerer, P.; Frielingsdorf, S.; Kroschinsky, S.; Friedrich, B.; Lenz, O.; Spahn, C. M. T. *Nature* **2011**, *479* (7372), 249–252.
- (9) Shomura, Y.; Yoon, K.-S.; Nishihara, H.; Higuchi, Y. *Nature* **2011**, *479* (7372), 253–256.
- (10) Volbeda, A.; Amara, P.; Darnault, C.; Mouesca, J.-M.; Parkin, A.; Roessler, M. M.; Armstrong, F. A.; Fontecilla-Camps, J. C. *Proc. Natl. Acad. Sci. U. S. A.* **2012**, *109* (14), 5305–5310.
- (11) Bowman, L.; Flanagan, L. A.; Fyfe, P. K.; Parkin, A.; Hunter, W. N.; Sargent, F. *Biochem. J.* **2014**, *458* (3), 449–458.
- (12) Frielingsdorf, S.; Fritsch, J.; Schmidt, A.; Hammer, M.; Löwenstein, J.; Siebert, E.; Pelmenchikov, V.; Jaenicke, T.; Kalms, J.; Rippers, Y.; Lendzian, F.; Zebger, I.; Teutloff, C.; Kaupp, M.; Bittl, R.; Hildebrandt, P.; Friedrich, B.; Lenz, O.; Scheerer, P. *Nat. Chem. Biol.* **2014**, *10* (5), 378–385.
- (13) Volbeda, A.; Charon, M.-H.; Piras, C.; Hatchikian, E. C.; Frey, M.; Fontecilla-Camps, J. C. *Nature* **1995**, *373* (6515), 580–587.
- (14) Rousset, M.; Montet, Y.; Guigliarelli, B.; Forget, N.; Asso, M.; Bertrand, P.; Fontecilla-Camps, J. C.; Hatchikian, E. C. *Proc. Natl. Acad. Sci. U. S. A.* **1998**, *95* (20), 11625–11630.
- (15) Ogata, H.; Kellers, P.; Lubitz, W. *J. Mol. Biol.* **2010**, *402* (2), 428–444.
- (16) Ogata, H.; Nishikawa, K.; Lubitz, W. *Nature* **2015**, *520* (7548), 571–574.
- (17) Gebler, A.; Burgdorf, T.; De Lacey, A. L.; Rüdiger, O.; Martinez-Arias, A.; Lenz, O.; Friedrich, B. *FEBS J.* **2007**, *274* (1), 74–85.
- (18) Greene, B. L.; Vansuch, G. E.; Wu, C.-H.; Adams, M. W. W.; Dyer, R. B. *J. Am. Chem. Soc.* **2016**, *138* (39), 13013–13021.
- (19) Dementin, S.; Burlat, B.; De Lacey, A. L.; Pardo, A.; Adryanczyk-Perrier, G.; Guigliarelli, B.; Fernandez, V. M.; Rousset, M. *J. Biol. Chem.* **2004**, *279* (11), 10508–10513.
- (20) Lukey, M. J.; Roessler, M. M.; Parkin, A.; Evans, R. M.; Davies, R. A.; Lenz, O.; Friedrich, B.; Sargent, F.; Armstrong, F. A. *J. Am. Chem. Soc.* **2011**, *133* (42), 16881–16892.
- (21) Goris, T.; Wait, A. F.; Saggi, M.; Fritsch, J.; Heidary, N.; Stein, M.; Zebger, I.; Lendzian, F.; Armstrong, F. A.; Friedrich, B.; Lenz, O. *Nat. Chem. Biol.* **2011**, *7* (5), 310–318.
- (22) Evans, R. M.; Parkin, A.; Roessler, M. M.; Murphy, B. J.; Adamson, H.; Lukey, M. J.; Sargent, F.; Volbeda, A.; Fontecilla-Camps, J. C.; Armstrong, F. A. *J. Am. Chem. Soc.* **2013**, *135* (7), 2694–2707.
- (23) Hexter, S. V.; Esterle, T. F.; Armstrong, F. A. *Phys. Chem. Chem. Phys.* **2014**, *16* (24), 11822–11833.
- (24) Murphy, B. J.; Sargent, F.; Armstrong, F. A. *Energy Environ. Sci.* **2014**, *7* (4), 1426–1433.

- (25) Fourmond, V.; Baffert, C.; Sybirna, K.; Lautier, T.; Abou Hamdan, A.; Dementin, S.; Soucaille, P.; Meynial-Salles, I.; Bottin, H.; Léger, C. *J. Am. Chem. Soc.* **2013**, *135* (10), 3926–3938.
- (26) Abou Hamdan, A.; Dementin, S.; Liebgott, P.-P.; Gutierrez-Sanz, O.; Richaud, P.; De Lacey, A. L.; Rousset, M.; Bertrand, P.; Cournac, L.; Léger, C. *J. Am. Chem. Soc.* **2012**, *134* (20), 8368–8371.
- (27) Roessler, M. M.; Evans, R. M.; Davies, R. A.; Harmer, J.; Armstrong, F. A. *J. Am. Chem. Soc.* **2012**, *134* (37), 15581–15594.
- (28) Marshall, N. M.; Garner, D. K.; Wilson, T. D.; Gao, Y.-G.; Robinson, H.; Nilges, M. J.; Lu, Y. *Nature* **2009**, *462* (7269), 113–116.
- (29) Stephens, P. J.; Jollie, D. R.; Warshel, A. *Chem. Rev.* **1996**, *96* (7), 2491–2514.
- (30) Mahadevi, A. S.; Sastry, G. N. *Chem. Rev.* **2013**, *113* (3), 2100–2138.
- (31) Liao, S.-M.; Du, Q.-S.; Meng, J.-Z.; Pang, Z.-W.; Huang, R.-B. *Chem. Cent. J.* **2013**, *7* (1), 44.
- (32) Kobayashi, K.; Mizuno, M.; Fujikawa, M.; Mizutani, Y. *Biochemistry* **2011**, *50* (44), 9468–9474.
- (33) Yorita, H.; Otomo, K.; Hiramatsu, H.; Toyama, A.; Miura, T.; Takeuchi, H. *J. Am. Chem. Soc.* **2008**, *130* (46), 15266–15267.
- (34) Xue, Y.; Davis, A. V.; Balakrishnan, G.; Stasser, J. P.; Staehlin, B. M.; Focia, P.; Spiro, T. G.; Penner-Hahn, J. E.; O'Halloran, T. V. *Nat. Chem. Biol.* **2008**, *4* (2), 107–109.
- (35) Sibert, R.; Josowicz, M.; Porcelli, F.; Veglia, G.; Range, K.; Barry, B. A. *J. Am. Chem. Soc.* **2007**, *129* (14), 4393–4400.
- (36) Dementin, S.; Belle, V.; Bertrand, P.; Guigliarelli, B.; Adryanczyk-Perrier, G.; De Lacey, A. L.; Fernandez, V. M.; Rousset, M.; Léger, C. *J. Am. Chem. Soc.* **2006**, *128* (15), 5209–5218.
- (37) Petrenko, A.; Stein, M. *Int. J. Mol. Sci.* **2017**, *18* (1), 100.
- (38) Petrenko, A.; Stein, M. *J. Phys. Chem. B* **2015**, *119* (43), 13870–13882.
- (39) Pershad, H. R.; Duff, J. L. C.; Heering, H. A.; Duin, E. C.; Albracht, S. P. J.; Armstrong, F. A. *Biochemistry* **1999**, *38* (28), 8992–8999.
- (40) Vincent, K. A.; Parkin, A.; Armstrong, F. A. *Chem. Rev.* **2007**, *107* (10), 4366–4413.
- (41) Vincent, K. A.; Cracknell, J. A.; Lenz, O.; Zebger, I.; Friedrich, B.; Armstrong, F. A. *Proc. Natl. Acad. Sci. U. S. A.* **2005**, *102* (47), 16951–16954.
- (42) Sharma, S.; Sivalingam, K.; Neese, F.; Chan, G. K.-L. *Nat. Chem.* **2014**, *6* (10), 927–933.
- (43) Bond, A. M.; Elton, D.; Guo, S.-X.; Kennedy, G. F.; Mashkina, E.; Simonov, A. N.; Zhang, J. *Electrochem. Commun.* **2015**, *57*, 78–83.
- (44) Adamson, H.; Robinson, M.; Bond, P. S.; Soboh, B.; Gillow, K.; Simonov, A. N.; Elton, D. M.; Bond, A. M.; Sowers, R. G.; Gavaghan, D. J.; Parkin, A. *Anal. Chem.* **2017**, *89* (3), 1565–1573.
- (45) Adamson, H.; Simonov, A. N.; Kierzek, M.; Rothery, R. A.; Weiner, J. H.; Bond, A. M.; Parkin, A. *Proc. Natl. Acad. Sci. U. S. A.* **2015**, *112* (47), 14506–14511.
- (46) Zhang, J.; Bond, A. M. *J. Electroanal. Chem.* **2007**, *600* (1), 23–34.
- (47) Léger, C.; Jones, A. K.; Albracht, S. P. J.; Armstrong, F. A. *J. Phys. Chem. B* **2002**, *106* (50), 13058–13063.
- (48) Tabares, L.; Gupta, A.; Aartsma, T.; Canters, G. *Molecules* **2014**, *19* (8), 11660.
- (49) Salverda, J. M.; Patil, A. V.; Mizzon, G.; Kuznetsova, S.; Zauner, G.; Akkiliç, N.; Canters, G. W.; Davis, J. J.; Heering, H. A.; Aartsma, T. *J. Angew. Chem., Int. Ed.* **2010**, *49* (33), 5776–5779.
- (50) Davis, J. J.; Burgess, H.; Zauner, G.; Kuznetsova, S.; Salverda, J.; Aartsma, T.; Canters, G. W. *J. Phys. Chem. B* **2006**, *110* (41), 20649–20654.
- (51) Morris, G. P.; Baker, R. E.; Gillow, K.; Davis, J. J.; Gavaghan, D. J.; Bond, A. M. *Langmuir* **2015**, *31* (17), 4996–5004.
- (52) Hidalgo, R.; Ash, P. A.; Healy, A. J.; Vincent, K. A. *Angew. Chem., Int. Ed.* **2015**, *54* (24), 7110–7113.
- (53) Murphy, B. J.; Hidalgo, R.; Roessler, M. M.; Evans, R. M.; Ash, P. A.; Myers, W. K.; Vincent, K. A.; Armstrong, F. A. *J. Am. Chem. Soc.* **2015**, *137* (26), 8484–8489.
- (54) Lu, M.; Compton, R. G. *Analyst* **2014**, *139* (10), 2397–2403.
- (55) Fourmond, V.; Infossi, P.; Giudici-Orticoni, M.-T.; Bertrand, P.; Léger, C. *J. Am. Chem. Soc.* **2010**, *132* (13), 4848–4857.
- (56) Mersch, D.; Lee, C.-Y.; Zhang, J. Z.; Brinkert, K.; Fontecilla-Camps, J. C.; Rutherford, A. W.; Reisner, E. *J. Am. Chem. Soc.* **2015**, *137* (26), 8541–8549.
- (57) Reeve, H. A.; Lauterbach, L.; Lenz, O.; Vincent, K. A. *ChemCatChem* **2015**, *7* (21), 3593–3593.
- (58) Pandelia, M.-E.; Nitschke, W.; Infossi, P.; Giudici-Orticoni, M.-T.; Bill, E.; Lubitz, W. *Proc. Natl. Acad. Sci. U. S. A.* **2011**, *108* (15), 6097–6102.
- (59) Pandelia, M.-E.; Bykov, D.; Izsak, R.; Infossi, P.; Giudici-Orticoni, M.-T.; Bill, E.; Neese, F.; Lubitz, W. *Proc. Natl. Acad. Sci. U. S. A.* **2013**, *110* (2), 483–488.
- (60) Flanagan, L. A.; Wright, J. J.; Roessler, M. M.; Moir, J. W.; Parkin, A. *Chem. Commun.* **2016**, *52* (58), 9133–9136.
- (61) Léger, C.; Bertrand, P. *Chem. Rev.* **2008**, *108* (7), 2379–2438.
- (62) Milton, R. D.; Abdellaoui, S.; Khadka, N.; Dean, D. R.; Leech, D.; Seefeldt, L. C.; Minter, S. D. *Energy Environ. Sci.* **2016**, *9* (8), 2550–2554.
- (63) Can, M.; Armstrong, F. A.; Ragsdale, S. W. *Chem. Rev.* **2014**, *114* (8), 4149–4174.
- (64) Suga, M.; Akita, F.; Hirata, K.; Ueno, G.; Murakami, H.; Nakajima, Y.; Shimizu, T.; Yamashita, K.; Yamamoto, M.; Ago, H.; Shen, J.-R. *Nature* **2015**, *517* (7532), 99–103.
- (65) Wright, J. J.; Salvadori, E.; Bridges, H. R.; Hirst, J.; Roessler, M. M. *J. Inorg. Biochem.* **2016**, *162*, 201–206.